Frequency and Field Variation of Vortex Dynamics in $YBa_2Cu_3O_{7-\delta}$

Dong Ho Wu, J. C. Booth, and Steven M. Anlage
Center for Superconductivity Research, Department of Physics, University of Maryland, College Park, Maryland 20742
(Received 8 March 1995)

We have measured the complex ac resistivity $\tilde{\rho}$ $(=\rho_1 + i\rho_2)$ of $YBa_2Cu_3O_{7-\delta}$ thin films in the frequency range of 45 MHz to 50 GHz. The microwave conductivity σ_1, obtained from $\tilde{\rho}$ in zero field, manifests considerable frequency dependence in the vicinity of T_c, showing that fluctuation and inhomogeneity effects are significantly reduced at high frequencies. With an applied dc magnetic field, the vortex dynamics changes at a crossover frequency f_x, showing scaling behavior $\rho_i \propto \omega^{\alpha_i}$ at low frequencies $(f < f_x)$ and mean-field behavior at high frequencies $(f > f_x)$.

PACS numbers: 74.25.Nf, 74.40.+k, 74.60.Ge, 74.72.Bk

In high temperature superconductors, the effects of thermal fluctuations are enhanced by several physical factors, such as the short coherence length, large penetration depth, higher temperature, and quasi-two-dimensionality. For the mixed state, in which magnetic flux penetrates a superconductor in quantized vortices, theoretical studies have proposed that these fluctuations, along with pinning disorder and interaction with other vortex lines, lead to a so-called vortex-glass state in the high temperature superconductors [1]. These proposals have been supported by several experiments [2–4]. In particular, recent experiments [3,4] demonstrated power-law behavior in the frequency dependence of the complex resistivity in the mixed state of $YBa_2Cu_3O_{7-\delta}$ (YBCO) thin films, supporting the vortex-glass based scaling model rather than the so-called mean-field models [5,6]. The experiments suggest that the scaling model yields the correct vortex behavior even at their highest measurement frequency (~600 MHz). However, this agreement needs to be reexamined more carefully at microwave frequencies and above because mean-field models are very successful in that range [7–9]. As the measurement frequency increases, the probing time scale becomes shorter, not allowing vortex lines enough time to interact with other vortices. Also it is known that at high frequencies, fluctuation effects become considerably smaller [10]. Consequently, one may expect that the scaling model is valid only up to a characteristic frequency. It has been suggested that if the measurement frequency exceeds a certain frequency range ($f \simeq 10^9 - 10^{11}$ Hz), intravalley oscillation of vortices plays the dominant role [11], implying that the interaction with other vortices can be ignored; hence, the scaling model may not be valid at high frequencies. These theoretical proposals have not been verified experimentally.

In this paper, we report a comprehensive experimental study on the field, temperature, and frequency dependence of the vortex dynamics of YBCO thin films at frequencies from 45 MHz to 50 GHz. The experimental results indicate that there is a crossover frequency f_x which falls within our measurement frequency range. Below f_x the scaling model provides a good description for the vortex dynamics, while above f_x the data follow rather a mean-field model description. The results suggest that at high frequencies the intravalley oscillation of vortices plays a dominant role for the ac dissipation, and mean-field models are appropriate.

The experiments are performed on six different c-axis YBCO thin films, all of which are approximately 1000 Å thick and fabricated by pulsed laser deposition on $LaAlO_3$ substrates. Although the experimental results vary somewhat with the degree of sample quality, the results reported here (obtained from sample III) were reproducible with different samples. The thin film is used to terminate a 0.086 in. diameter, 50 Ω coaxial transmission line, and the effective surface impedance Z_s^{eff} is obtained from swept frequency measurements of the complex reflection coefficient using an HP8510C vector network analyzer [12]. This geometry, in which the currents [13] flow only radially between the inner and outer conductors, is referred to as the Corbino geometry, and is beneficial when studying vortex motion, because the edges of the sample are effectively eliminated and do not contribute to the creation and/or pinning of vortices. A variable magnetic field (0–9 T) is applied parallel to the c axis of the sample by means of a superconducting Nb-Ti magnet, which requires the transmission line to be ~2 m long. To eliminate the effects of the transmission line and test set from the measurement, we employ a calibration scheme as described in Ref. [12]. Measurements have also been performed using a much shorter length transmission line (~6 cm) in a setup with a small magnetic field (≲0.5 T) provided by CoSm magnets, and similar results were obtained.

Under conditions where the film thickness t_0 is much less than the penetration depth, the measured surface impedance is given simply by $Z_s^{\text{eff}} \simeq \tilde{\rho}/t_0$ where $\tilde{\rho}$ $(=\rho_1 + i\rho_2)$ is the complex resistivity [12]. The transition width of ρ_1 is ~1 K, much broader than those of high quality single crystals. The broad transition of $\rho_1(T)$ reflects the existence of disorder which is typically unavoidable in thin film samples. Also $\rho_1(T)$ indicates that

0031-9007/95/75(3)/525(4)$06.00

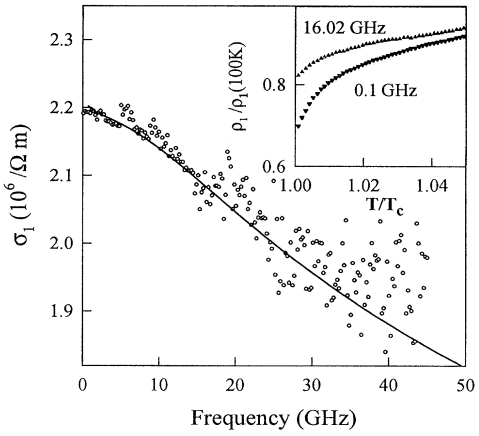

FIG. 1. The frequency dependence of $\sigma_1(T)$ at $T = 88.2$ K. Inset: rounding near the onset of the transition in $\rho_1/\rho_1(100\ \mathrm{K})$ at 16.02 and 0.1 GHz.

rounding near the onset of the transition becomes smaller at higher frequencies (see the inset of Fig. 1), suggesting the fluctuation contribution to the conductivity σ becomes smaller at high frequencies. Using $\tilde{\rho} = 1/(\sigma_1 - i\sigma_2)$, we extract σ_1 and σ_2, which reveal considerable frequency dependence. In particular, as shown in Fig. 1, $\sigma_1(\omega)$ exhibits larger conductivity at low frequencies and decreases significantly at high frequencies. The solid line in Fig. 1 represents $\sigma_1(\omega) = k[\sigma_1^{\mathrm{EM}}(\omega) + \sigma_1^{F}(\omega)]$, where $\sigma_1^{\mathrm{EM}}(\omega)$ is the real part of the effective conductivity calculated using an effective medium model [14] to account for the sample inhomogeneity, and $\sigma_1^{F}(\omega)$ is a calculation of the fluctuation conductivity with an effective dimensionality $D = 3$, based on the time-dependent Ginzburg-Landau theory [15]. The best fit is obtained using the parameters $\xi_0 \simeq 3$ Å, $T_c = 88.35$ K, and $\delta T_c = 1.1$ K and the prefactor value $k \sim 0.8$. Figure 1 illustrates that the effect of fluctuations and inhomogeneity are greatly diminished with increasing frequency.

Below T_c, these inhomogeneities will act as a disordered pinning potential for vortices. It is expected that the fluctuation and disorder effects destroy the crystalline long-range order of the vortex lattice phase, leading to the vortex glass state at and below a characteristic temperature T_g, as supported by experiments at frequencies $f \lesssim 600$ MHz [2–4]. Increasing the frequency reduces the excursion of the vortices, not allowing time to probe the disordered barriers; hence, the disorder plays less of

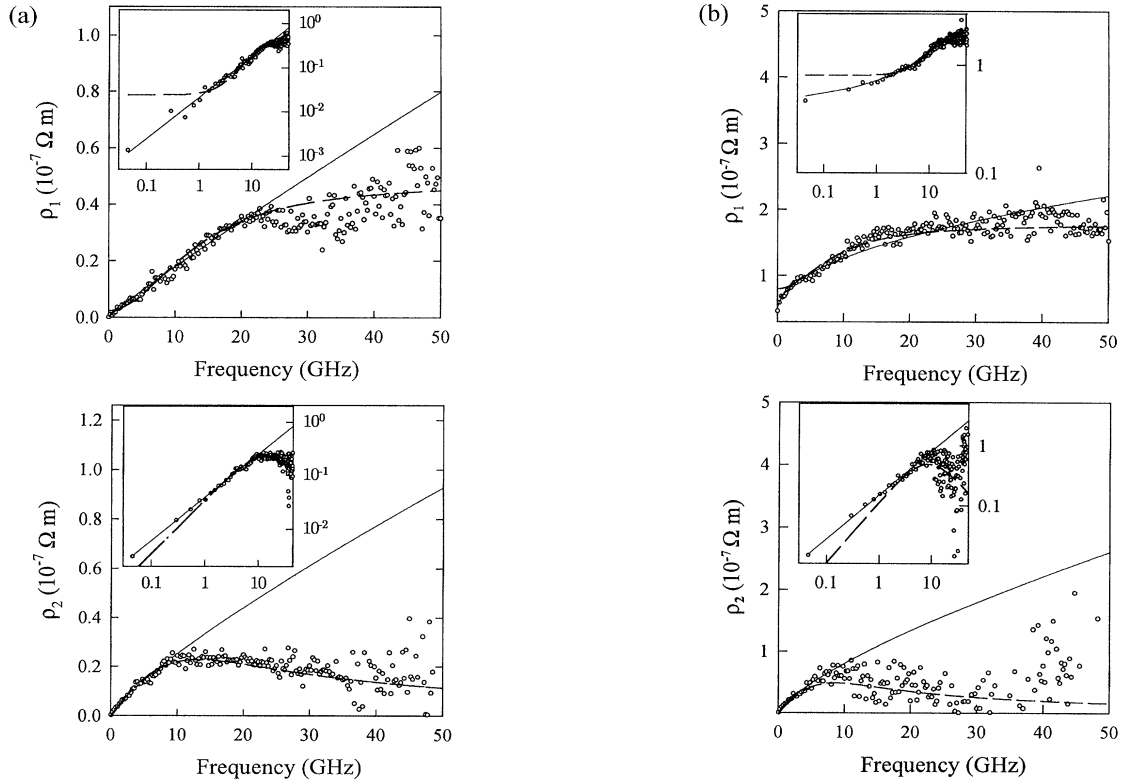

FIG. 2. The frequency dependence of $\rho_1(\omega)$ and $\rho_2(\omega)$. (a) For $T = 80.2$ K and $H = 0.4$ T, the solid lines represent $\rho_1 \propto \omega^{\alpha_1}$ and $\rho_2 \propto \omega^{\alpha_2}$. (b) For $T = 83.6$ K and $H = 4$ T, the solid lines display $\rho_1 = \rho_0 + a_1\omega^{\alpha_1}$ and $\rho_2 \propto \omega^{\alpha_2}$. The dashed lines in both figures represent the mean-field fit.

a role. Similar experiments over an extended frequency range (45 MHz $\leq f \leq$ 50 GHz) are necessary to examine the validity of the scaling model at high frequencies. Figures 2(a) and 2(b) exhibit typical frequency dependence of ρ_1 and ρ_2 obtained at $T = 80.2$ K with $H_{dc} = 0.4$ T and at $T = 83$ K with $H_{dc} = 4$ T, respectively. To verify a universal power-law behavior, we plot both $\rho_1(\omega)$ and $\rho_2(\omega)$ on a log-log scale (see the inset of Fig. 2). We find that $\rho_1 \propto \omega^{\alpha_1}$ and $\rho_2 \propto \omega^{\alpha_2}$ with $\alpha_1 \simeq 0.93$ and $\alpha_2 \simeq 0.81$ in Fig. 2(a), showing vortex "solid" behavior, until the measurement frequency reaches a characteristic value ($f_x \sim 8-9$ GHz, as explained later). For Fig. 2(b), the data can be described by a modified power law $\rho_1 = \rho_0 + A\omega^{\alpha_1}$ and $\rho_2 \propto \omega^{\alpha_2}$, showing vortex "liquid" behavior, again until the frequency reaches a characteristic frequency. Overall the data for $f < f_x$ follow the power-law frequency dependence, as the scaling model predicts, with $0.45 \leq \alpha_1 < 1$ and $0.7 \leq \alpha_2 < 1$ over the temperature ($78 \leq T \leq 86$ K) and the field ($0.3 \leq H \leq 4$ T) range. The results are consistent with those of Ref. [4] to within ~10%. Above the characteristic frequency, the data follow rather a mean-field type behavior, as represented by the dashed lines. The fits are made using a mean-field model $\tilde{\rho} = \rho_f[\epsilon + (\omega\tau)^2 + i(1-\epsilon)\omega\tau]/[1 + (\omega\tau)^2]$ with the adjustment of the values of the flux flow resistivity ρ_f, the flux creep factor ϵ, and the characteristic vortex relaxation time τ to yield the best fit to the data [6]. Thus it appears that to describe $\tilde{\rho}(\omega)$ over the whole frequency range (45 MHz $\leq f \leq$ 50 GHz) we need to use each model for two different frequency regimes: the scaling model for low frequencies and the mean-field type model for high frequencies. This tendency is obvious for the vortex solid state, while it is less clear for the vortex liquid state.

A quantity that can be used to locate the vortex behavior crossover is the phase angle ϕ defined by $\tilde{\rho} = |\rho|e^{i\phi}$, so that $\phi = \tan^{-1}(\rho_2/\rho_1)$. We find that for $T > T_c$ the phase angle $\tan\phi \sim 0$ with the absence of frequency dependence. As temperature decreases below T_c, $\phi(\omega)$ increases at low frequencies, and the frequency dependence becomes obvious, consistent with the results of Ref. [3]. Figure 3 shows the frequency dependence of $\tan\phi$ for $T < T_c$. At low frequencies, $\tan\phi$ decreases or increases with frequency and enters into a plateau regime. In general our results are consistent with those of Wu, Ong, and Li [4] which revealed that $d\phi/d\omega > 0$ in the vortex liquid state, $d\phi/d\omega \simeq 0$ and $\phi_c \simeq 65.7° \pm 2°$ at the critical point, and $d\phi/d\omega < 0$ in the vortex solid state. We find somewhat different critical phase angle values ϕ_c in our experiments: Sample III with $H_{dc} = 0.3$ T reveals $\phi_c \simeq 63° \pm 5°$ at $T_g \simeq 86$ K, while sample V with $H_{dc} \lesssim 0.1$ T exhibits $\phi_c \simeq 75° \pm 5°$ at $T_g \simeq 83.1$ K. The frequency dependence of $\phi(\omega)$ described above is valid for low frequencies. With further increase of frequency, all the data show $\tan\phi \propto 1/\omega$, suggesting the change of vortex dynamics from the scaling to mean-field behavior, and thus identifying the crossover frequency f_x (e.g., $f_x \simeq 8-9$ GHz for $H_{dc} = 0.4$ T and $T = 80.2$ K) which demarcates the region of scaling behavior and the mean-field behavior.

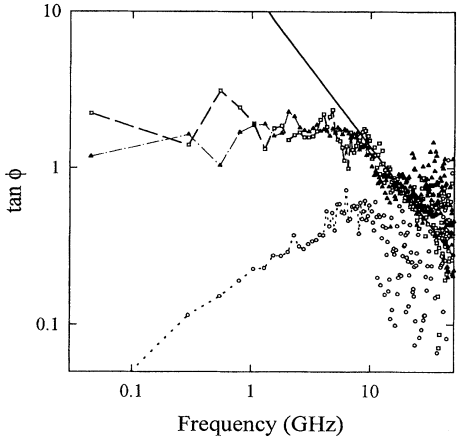

FIG. 3. The phase angle $\tan\phi = \rho_2/\rho_1$ vs frequency for various temperatures and field strengths. Dashed line: $T = 80.2$ K, $H = 0.4$ T. Dash-dotted: $T = 86$ K, $H = 0.3$ T. Dotted: $T = 83$ K, $H = 4$ T. Solid line represents $\tan\phi \propto 1/\omega$ at high frequencies.

The characteristic vortex relaxation time τ, which is determined by the interplay between elastic and viscous forces, is obtained from the mean-field fit for the high frequency data. At $T = 78$ K and $H_{dc} = 0.3$ T, the fit yields $1/\tau \simeq 13 \times 10^9$ sec^{-1}, somewhat larger than our earlier result from YBCO single crystals ($1/\tau_{xtal} \simeq 9.6 \times 10^9$ sec^{-1}) [16]. We find that ϵ increases with temperature and magnetic field strength within the range $0.05 < \epsilon \leq 0.5$ for $80 < T < 86$ K and $0 < H_{dc} < 1$ T. Using the value of ρ_f (obtained from the fit) and the relation $\rho_f = B\phi_0/\eta$, we extract $\eta \simeq 2 \times 10^{-8}$ N sec/m^2 for $T = 80.2$ K and $H_{dc} = 0.4$ T, showing a reasonable agreement with our earlier results [8,16].

Geshkenbein *et al.* [11] proposed that the nature of the ac vortex motion can be distinguished by two essentially different regimes: intravalley oscillations and intervalley transitions. For the intravalley oscillations, the vortices move individually and the motion is dominantly confined within the random pinning potential well, whereas for the intervalley transitions the vortices move collectively and the vortex motion is dominated by thermally activated hops between different metastable states in the random pinning potential. Our estimated f_x falls within the predicted microscopic frequency range (~10^9-10^{11} Hz) of the intravalley oscillations, implying that the crossover from the scaling behavior to the mean-field-like behavior is related to the crossover from the intervalley transitions to intravalley oscillations.

The nature of vortex motion can be explored also from the detailed shape of the ρ_1-H_{dc} curves. Figure 4 displays

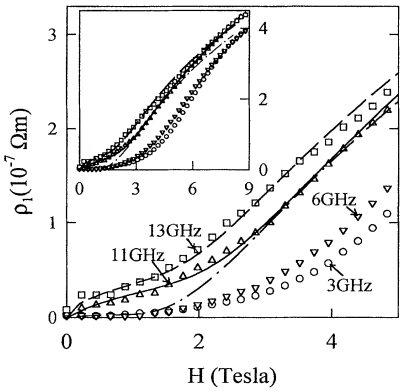

FIG. 4. Field dependence of $\rho_1(H)$ for various frequencies at $T = 83.5$ K. Dash-dotted line is a mean-field fit for 3 GHz. Solid line and dashed line are mean-field fits for 11 and 13 GHz, respectively. Inset: $\rho_1(H)$ for $0 \leq H \leq 9$ T.

some of the field dependent $\rho_1(H)$ measured at $T = 83.5$ K, along with mean-field fits. The data measured at 11.04 and 13.03 GHz follow the mean-field description of $\rho_1(H)$ at all fields [7]. For the mean-field fit, we used the full expressions for $\tau = (\eta/\kappa_p)[\{I_0^2(\nu) - 1\}/I_1(\nu)I_0(\nu)]$ and $\tilde{\rho}$ (given above and in Ref. [6]) with variables $\nu = H^*/H$ and $\epsilon = I_0(\nu)^2$. Here $I_0(\nu)$ is a modified Bessel function of zeroth order. We adjusted the field scale H^*, the viscosity η, and the pinning force constant κ_p as fitting parameters. The best fits are obtained with the values given in Table I. The values for η and κ_p are comparable to our earlier results [8,16] and also those extracted from $\tilde{\rho}(\omega)$. In contrast to the high frequency data, the low frequency data ($f = 2.99$ and 5.97 GHz) cannot be reconciled with the mean-field fit with reasonable parameter values. It seems that the onset of dissipation of the low frequency data is much smoother than what we can obtain from the mean-field model, and it resembles the E-J curves of the scaling models proposed by Fisher, Fisher, and Huse [1]. Hence, the results of $\rho_1(H)$ also suggest that the vortex behavior changes dramatically with frequency.

TABLE I. The parameter values for the mean-field fits in Fig. 4.

Frequency (GHz)	H^* (T)	η (N sec/m^2)	κ_p (N/m^2)
2.99	3.6	3.2×10^{-8}	2.5×10^3
11.04	3.6	3.2×10^{-8}	3.5×10^3
13.03	3.5	3.5×10^{-8}	4.5×10^3

In summary, through the measurements of the complex resistivity with frequency and field variation, we demonstrate that the behavior of vortex dynamics changes dramatically at a crossover frequency. Below the crossover frequency, the experimental results are consistent with the scaling behavior, suggesting collective vortex motion, while above the crossover frequency, experiments show consistency with mean-field type pinning-dominated behavior until the frequency becomes comparable to the "depinning frequency" $1/\tau$ above which the mean-field type viscous motion dominates. Our results demonstrate the importance of a new characteristic time scale, in addition to length scales [1], in developing appropriate models for vortex dynamics in superconductors.

We thank C. J. Lobb and R. L. Greene for stimulating discussions and A. Findikoglu and C. Kwon for assistance with sample preparation. This work was supported by the NSF NYI Grant No. DMR-9258183.

[1] D. S. Fisher, M. P. A. Fisher, and D. A. Huse, Phys. Rev. B **43**, 130 (1991).
[2] R. H. Koch *et al.*, Phys. Rev. Lett. **63**, 1511 (1989).
[3] H. K. Olsson *et al.*, Phys. Rev. Lett. **66**, 2661 (1991).
[4] Hui Wu, N. P. Ong, and Y. Q. Li, Phys. Rev. Lett. **71**, 2642 (1993).
[5] J. I. Gittleman and B. Rosenblum, Phys. Rev. Lett. **16**, 734 (1966).
[6] M. W. Coffey and J. R. Clem, Phys. Rev. Lett. **67**, 386 (1991).
[7] J. Owliaei, S. Sridhar, and J. Talvacchio, Phys. Rev. Lett. **69**, 3366 (1992).
[8] M. S. Pambianchi *et al.*, IEEE Trans. Appl. Supercond. **3**, 2774 (1993).
[9] E.-J. Choi *et al.*, Phys. Rev. B **49**, 13 271 (1994).
[10] S. L. Lehoczky and C. V. Briscoe, Phys. Rev. B **4**, 3938 (1971).
[11] V. B. Geshkenbein *et al.*, Phys. Rev. B **43**, 3748 (1991).
[12] J. Booth, Dong Ho Wu, and S. M. Anlage, Rev. Sci. Instrum. **65**, 2082 (1994).
[13] The current density is estimated to be $2 \times 10^2 - 8 \times 10^1$ A/cm^2 and is far smaller than a typical critical current density $(3-5) \times 10^6$ A/cm^2 at 77 K (or $\sim 10^5$ A/cm^2 at 86 K).
[14] A. A. Golubov *et al.*, Physica (Amsterdam) **213C**, 139 (1993); D. Walker and K. Scharnberg, Phys. Rev. B **42**, 2211 (1990).
[15] H. Schmidt, Z. Phys. **232**, 443 (1970).
[16] Dong Ho Wu and S. Sridhar, Phys. Rev. Lett. **65**, 2074 (1990).